A 2D Ultrasonic Phased Array Optimization Framework Enabled by Reconfigurable Laser Induced Phased Arrays

Journal of Physics: Conference Series **2822** (2024) 012094 doi:10.1088/1742-6596/2822/1/012094

A 2D Ultrasonic Phased Array Optimization Framework Enabled by Reconfigurable Laser Induced Phased Arrays

Peter Lukacs*, Geo Davis, Don Pieris, Theodosia Stratoudaki

Electronic and Electrical Engineering, University of Strathclyde, 204 George Street, Glasgow G1 1XW, UK.

Peter.lukacs@strath.ac.uk

Abstract. Three-dimensional (3D) ultrasonic imaging enables the viewing of internal features in a more accurate way than cross-sectional imaging. 3D imaging requires two-dimensional (2D) ultrasonic phased arrays to resolve all three spatial dimensions through beamforming along azimuthal and elevation angles. 2D phased arrays pose a manufacturing and control challenge due to the requirement of large number of elements to satisfy the Nyquist sampling limit. This problem can be alleviated through the use of sparse ultrasonic array designs. The optimization process is critical, as this dictates the efficiency of suppression of grating lobes. The aim of this work is to establish a framework for design of optimized sparse 2D phased arrays. This is enabled by exploiting the reconfigurability of Laser Induced Phased Arrays (LIPAs). LIPAs are synthetic arrays produced by scanning one laser for ultrasound generation and another for ultrasound detection, independently of each other. The reconfigurability and decoupled ultrasonic generation and detection of this systems enables easy and fast implementation of any arbitrary array layout. The framework consists of an analytical model for parametric evaluation of designs. The model performs a parametric sweep on the generation and detection element positions for each array design in order to identify the optimal parameters, based on mean and maximum side-lobe level. In the presented framework, four array designs are utilized for the optimization process: matrix, random, Vernier and a novel array design the Rotated Array (RA).

1. Introduction

Ultrasonic waves are widely used to probe the insides of optically opaque objects. Images can also be created using these waves in order to assess certain qualities of these objects. Commonly, the images produced are cross-sectional, two-dimensional (2D), representing a single slice of the object. The object and its internal features are volumetric, thus viewing them through cross-sectional images is not always representative of the object, because it assumes that the object does not vary in the dimension normal to the plane of the image. Three-dimensional (3D) imaging offers a way to produce a more accurate view of internal features, as the variance of the feature can be represented in all three spatial dimensions.

Ultrasonic imaging is performed using ultrasonic phased array, consisting of multiple elements. The elements can be physically placed in an array or a single element is mechanically scanned, where beam steering and focusing is achieved in post-processing, in which case the array is synthetic. 2D images can be produced using 1D arrays and 3D images can be produced, either by using a 2D arrays[1], or by scanning a 1D array normal to the array axis and then stacking the multiple 2D images to produce a 3D image. 2D arrays offer clear advantages over 1D arrays in terms of ultrasonic imaging. Stacking 2D images in order to produce a 3D image leaves one of the dimensions unresolved, while using 2D arrays for 3D imaging is superior, as they resolve all three dimensions. Furthermore, internal features,

depending on their shape, size and orientation, can reflect ultrasound away from the plane of imaging when using a 1D array, which results in these features not being imaged. This is not the case for 2D arrays as they detect ultrasound waves over an area of the surface rather than just in a line.

However, a 2D array with aperture size comparable to that of a 1D array, requires significantly more elements. If the interelement spacing is the same for the 1D and the 2D array, the former will have n elements, while the latter $n \times n$ elements. This poses a challenge in: array manufacturing; controlling instrumentation; processing and storage of the corresponding large data sets. Reducing the number of elements while keeping the aperture constant can lessen this problem, however once the interelement spacing becomes large enough to exceed the Nyquist sampling limit (i.e.: the interelement spacing becomes larger than half the acoustic wavelength), the array becomes sparse and grating lobes appear that deteriorate the imaging quality and can result in imaging artefacts [2]. These grating lobes appear due to the periodic sampling points (element positions) of the array and their amplitude can be reduced through various means such as by placing the elements in a non-periodic arrangement [3].

There is a great interest in optimizing sparse arrays to enable the design of cheaper and easier-to-control 2D arrays without producing artefacts, therefore making 3D imaging easier to implement for application by end-users [4,5]. The most commonly used ultrasonic phased arrays consist of piezo-electric transducers, where the array design is defined during manufacturing. In order to experimentally optimize sparse arrays either a new array with the optimized design has to be manufactured [4] or a set number of elements of a very large array has to be addressed [5]. The former can be expensive and slow, while the later can limit the optimization process to an already defined layout.

An alternative array technology to transducer-based arrays is Laser Induced Phased Arrays (LIPAs), where ultrasound is generated and detected by lasers and the array is produced by scanning a single generation and a single detection laser independently of each other [6]. Utilizing such an acquisition method allows for changing the array parameters, such as number of elements and their position, thus prototyping and experimentally evaluating different sparse array designs can be done rapidly without the need to manufacture new instruments.

Recently 2D LIPAs have been experimentally demonstrated proving that 3D imaging can be achieved with LIPAs [7]. Furthermore, optimized array designs have also been experimentally implemented showing that sparse 2D LIPAs can be utilized without inducing high amplitude artefacts [8]. This demonstration showed the potential of LIPAs for prototyping 2D ultrasonic arrays. In the present work, an optimization process is developed for sparse 2D LIPAs. In this process three designs are evaluated, the Vernier, random and a novel array design, the rotated array and each of these designs is compared to the performance of a matrix array. The designs are assessed by means of an analytical model which calculates the theoretically array directivity of the specific array design. The performance of each array design is evaluated based on the grating lobe and side lobe amplitudes in the array directivity.

2. Design Optimisation Process

This section details the process of 2D array design optimisation, and it consists of three sections: 1) the analytical model which can calculate the performance of arrays, 2) description of the array designs considered in this work and 3) the parametric sweep applied to the designs for optimisation.

2.1. Analytical Model

In this section the analytical model that was used to evaluate the performance of the different array designs is described. This model considers the contribution of individual array elements to the overall acoustic field produced, according to the focusing capabilities of LIPAs. This acoustic field is then describing the directivity of the array when focusing for a specific point, thus providing information about the amplitude observed at the focal point and away from it. The equation for calculating the acoustic field produced by single array element for a pixel located at (x,y,z) is calculated using the following equation:

$$P_n(x, y, z) = Be^{i(kr-\omega t)}$$

Where *r* is the distance between the array element and the pixel, k is the wavenumber, ω is the phase delay applied to that element and B is the geometrical attenuation of the ultrasonic wave. This attenuation can be defined for spherical waves by:

$$B = \frac{1}{r}$$

The data acquisition process consists of capturing an ultrasonic signal for each generation and detection array element combination. This is called the Full Matrix Capture (FMC) acquisition process. The image processing algorithm applied to these signals is called the Total Focusing Method (TFM), which focuses on every pixel of the image by delaying and summing all the signals according to the calculated ultrasonic ray paths [9]. This algorithm thus achieves focusing both in transmission and reception. The acoustic field produced for a pixel can then be described as

$$P_{total}(x,y,z) = \sum_{n=1}^{N} P_{Tx} \sum_{n=1}^{N} P_{Rx}$$

Where N is the total number of array elements and P_{Tx} and P_{Rx} are the fields produced in transmission and reception, respectively. The directivity patterns of laser generated and detected ultrasound and their effects must be taken into account when calculating the acoustic field produced by the array, as follows

$$P_{Tx}(x,y,z) = G(\Theta)Be^{i(kr-\omega t)}$$
$$P_{Rx}(x,y,z) = D(\Theta)Be^{i(kr-\omega t)}.$$

The generation and detection directivity patterns G and D are described in [6] and the angle Θ is the angle relative to the surface normal at the position of the elements and is defined as a function of (x,y,z) coordinates of the given pixel. The directivity can be utilised for shear or longitudinal modes. In this study the shear wave mode is considered.

The acoustic field is calculated for a specific focus point in mind, along a constant distance from the centre of the array, which is the distance to the focal point. This produces values for the pressure field along a semi-sphere as a function of elevation and azimuthal angles. In order to visualise the results on a 2D graph, the polar, 3D space is converted onto a 2D, U-V space by performing U-V mapping, where the two axes are defined by:

$$u = \sin(\Theta)\cos(\varphi)$$
$$v = sin(\Theta)sin(\varphi)$$

Where Θ and φ are the elevation and azimuthal angles.

2.2. Array designs

In this work four array designs are considered: the matrix array, the Vernier array, the random array and the rotated array. An example array for each design is shown in figure 1.

The matrix array design, shown on figure 1 (A), has the same layout for generation and detection elements, with a constant pitch in both the dimensions of the array. The Vernier array, shown on figure 1 (B), has different interelement spacing for the generation and detection arrays, however this spacing for the individual arrays is constant in both dimensions. This is either achieved by having a different number of generation and detection elements, while having the same aperture size (this is the example shown in figure 1 (B)), or same number of generation and detection elements, with differing aperture sizes (this is the approach utilized in the optimization process described in sections 2.3 and section 3). The random array, shown in figure 1 (C), has the same number of elements and positions for the generation and detection arrays, however the elements are located randomly within the aperture. The randomness is introduced by initially starting with the matrix array, and a value of randomness is applied in both dimension to each element of the array. The rotated array, shown on figure 1 (D), has the same number of elements in the generation and detection arrays and initially their positions are identical. Then the centre of one array (e.g. the generation array) is rotated relative to the centre of the other array (e.g. the detection array).

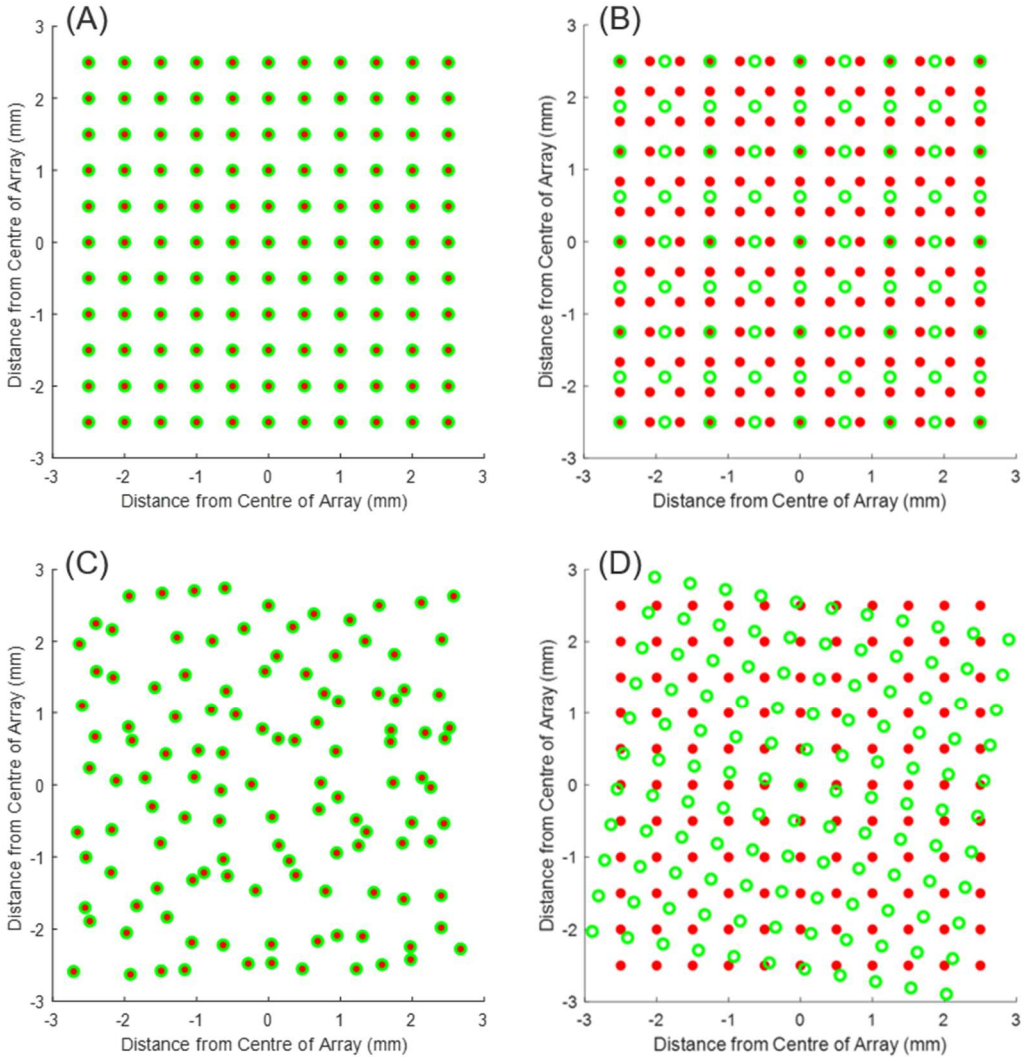

Figure 1. Array designs: (A) matrix array, (B) Vernier array, (C) random array, (D) rotated array. Green circles and red dots indicate position of detection and generation elements in the array, respectively.

The array directivity of these designs can be analytically calculated as described in section 2.1. Figure 2 shows the resulting array directivities, using the same array parameters presented in figure 1, while focusing 5.5 mm deep, below the array centre. The calculations were performed for a frequency value of 8 MHz. For each array the array directivity produced by the generation and the detection arrays are individually plotted along with the combined directivity. Each figure was normalized to their respective maximum value and converted to a logarithmic scale.

The graphs in figure 2 show the array directivity when focusing to a specific point. The main lobe can be observed at the same point on each figure, which is red point in the middle of each figure, highlighted by the white arrow on figure 1 (A). The side lobes can be observed near the main lobe, one of which has been highlighted by a red arrow on figure 1 (A). Finally, the grating lobes can be seen towards the edges of the figures. The green arrow in figure 1 (A) shows an example of a grating lobe.

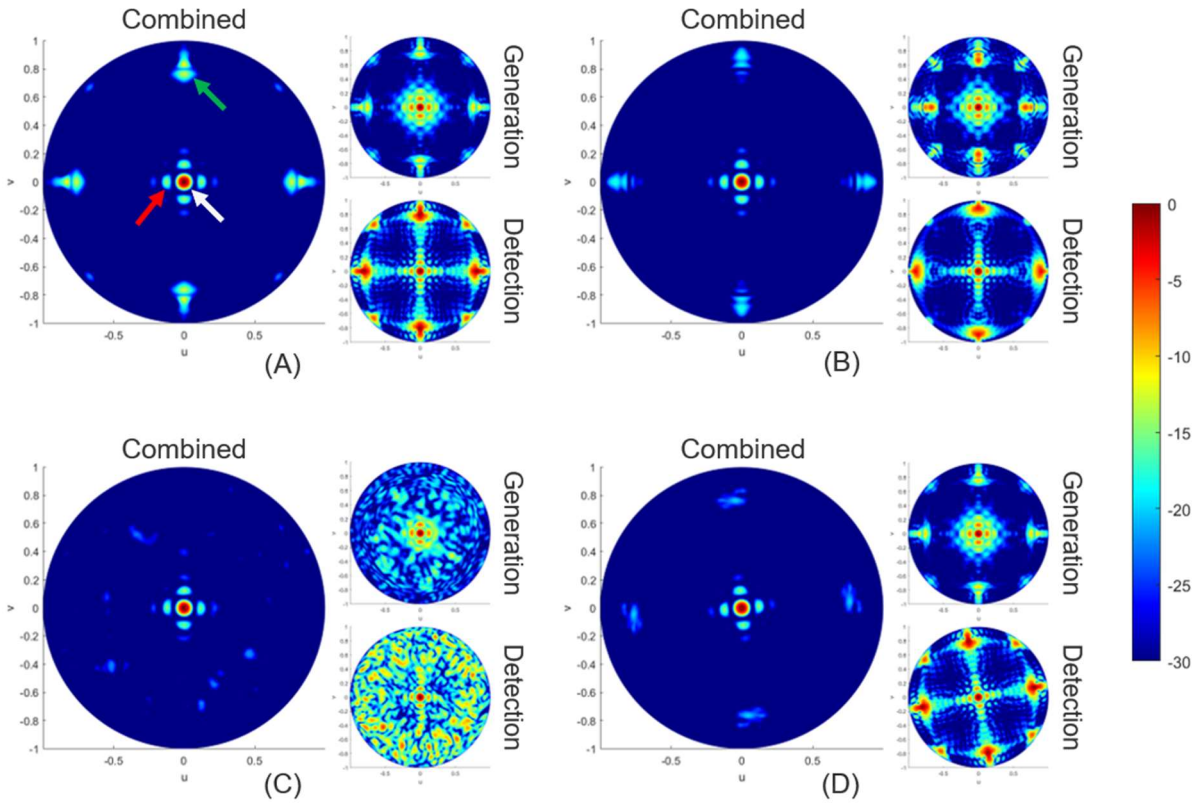

Figure 2. Array directivity of the (A) matrix array, (B) Vernier array, (C) random array, (D) rotated array. White, red and green arrows point to the main lobe, a side lobe and a grating lobe respectively.

2.3. Optimisation Process and Parameters

A different optimisation process was utilised for each design, with the exception of the matrix array, for which no optimisation was carried out. For each design the maximum grating lobe and the mean grating lobe levels are measured from the calculated analytical array directivity as a certain design parameter is varied. Selecting the design parameter that produces the lowest values for maximum and mean grating lobes provides the optimised design. The common parameters for each design was the number of array elements, which was 121 generation and 121 detection elements.

The optimization process for the Vernier array consists of gradually changing the interelement spacing of either the generation or detection array, while keeping the interelement spacing and the number of elements of the other array constant. In this study the generation pitch was changing, starting with 260 μm, increasing in steps of 10 μm for a total of 100 increments. The detection pitch was constant, at 500 μm in both dimensions.

The optimization of the random array is carried out by applying various random array designs. The randomness applied in each dimension was limited in this study to ± 0.5 times the interelement spacing. Overall 100 random designs were applied.

Optimization for the rotated array is done by changing the rotation angle between the two arrays. The rotation was carried out in steps of 1 degree, from 0 to 90 degrees. Higher degrees were not considered in this study as this would repeat or mirror the previously realized array designs.

3. Results and Discussion

This section presents the grating lobe values obtained while varying the design parameters, described in subsection 2.3, and the relevant discussion. As a benchmark, the results are compared to the performance of the matrix array, which had maximum and mean grating lobe values of -2.22 dB and -58.97 dB

respectively. The array directivities were calculated for a frequency of 5 MHz and a focal point located at 15 mm deep and 5 mm away from the center of the array in the other two dimensions.

Figure 3 (A) and (B) show the maximum and mean grating lobe values for the Vernier array as a function of the ratio of generation to detection interelement spacing. When this ratio is one, the design is equivalent to the matrix array. Applying a different interelement spacing for generation and detection arrays results in different levels of sparsity, thus the grating lobes of one array will appear at different angles relative to the grating lobes of the other (see figure 2 (B)). The two peaks appearing in figure 3 (A) can be explained by this. The largest maximum grating lobe value appears when the ratio of the generation to detection interelement spacing is 1, as this is when the grating lobes appear at the same angles. When the ratio becomes 2, the next order grating lobes from the sparser array (i.e.: either the generation or the detection array) will appear at the same angles as the grating lobes of the less sparse array.

The lowest maximum grating lobe value achieved is -21.56 dB, when the generation to detection interelement spacing ratio is 1.56. As the overall sparsity of the array is increasing, the mean grating lobe value is also increasing. At this generation to detection interelement spacing ratio (i.e.: 1.56) the corresponding mean grating lobe value is -52.91 dB.

Logically, the lowest possible mean grating lobe level is achieved when the lowest sparsity is used, that is when the interelement spacing is the smallest. At this point the mean grating lobe is -65.79 dB and the corresponding maximum grating lobe value is -18.47 dB. However, it must be noted that at this point, due to keeping the number of array elements constant, the generation array has an aperture half the size of the detection array. Thus, a disadvantage of this design is that it will lead to a decrease in imaging resolution, as lateral resolution is mainly dictated by the array aperture size.

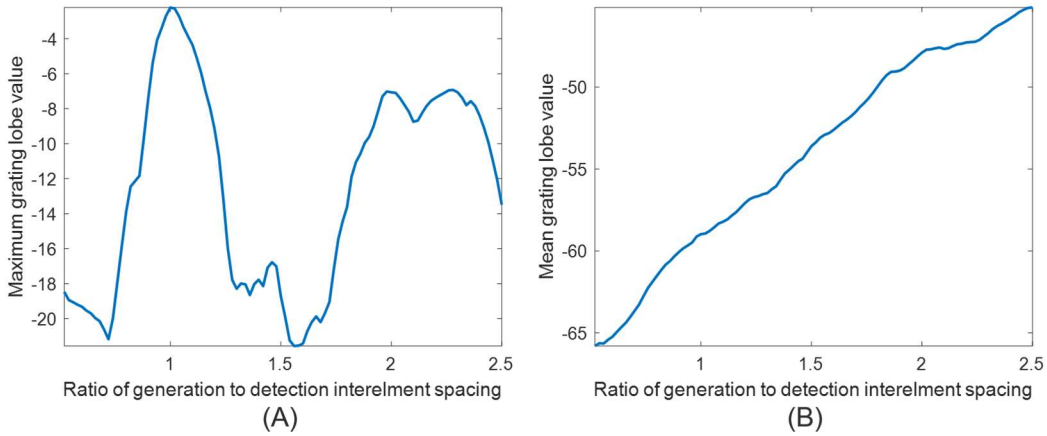

Figure 3. (A) Maximum and (B) mean grating lobe levels from the array directivity calculated for the Vernier array optimisation. Y axis units are in dB.

Figure 4 (A) and (B) show the maximum and mean grating lobe levels for the random array, respectively. For this design, the variance in maximum and mean grating lobe levels is much lower than in the previous case and a particular trend is not observed as the design is randomly varied. The optimization of the random array is challenging due to this random variance as there is no controllable design parameter. The lowest maximum grating lobe level is achieved when using random design number 33, which is -21.99 dB, with a corresponding mean grating lobe level of -48.43 dB. While the lowest mean grating lobe level is -49.85 dB, for the random design number 26, which has a corresponding maximum grating lobe level of -19.51 dB. Overall, the mean grating lobe values appear to be larger than that of the matrix array by around 10 dB on average. However significant improvement is achieved in maximum grating lobe levels.

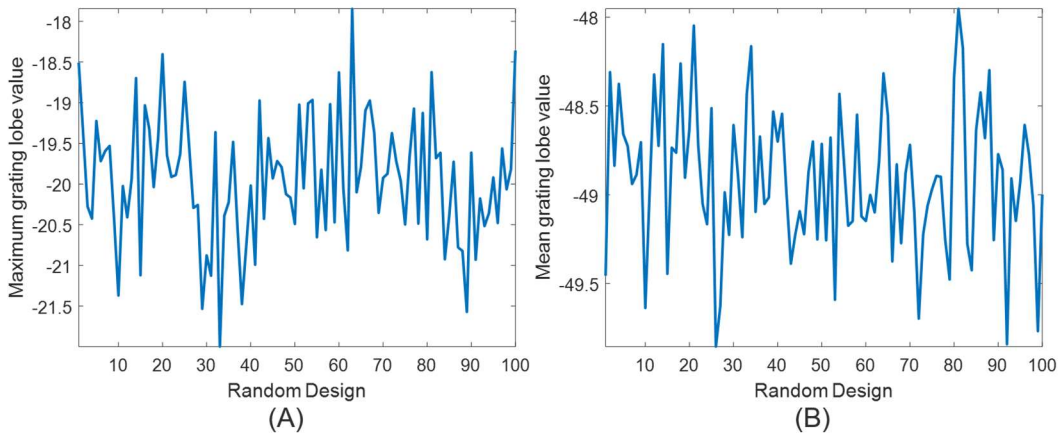

Figure 4. (A) Maximum and (B) mean grating lobe levels from the array directivity calculated for the random array optimisation. Y axis units are in dB.

Figure 5 (A) and (B) show the maximum and mean grating lobe levels for the rotated array, respectively. An array identical to the matrix array is achieved when 0-degree rotation is applied. Applying a 90-degree rotation produces an array which is identical to the starting array (i.e.: 0-degree rotation), due to the two orthogonal lines of symmetry of the array design. The graphs in figure 5 are symmetrical to the 45-degree point, as for example a 60-degree rotation is the same as applying a 90 minus 60-degree rotation, thus producing the same result as when applying a 30-degree rotation. Overall the design performs worst when no rotation is applied. At higher angles the grating lobes produced by the generation and detection arrays no longer align with each other (see figure 2 (D)), due to the rotation. The lowest maximum grating lobe level, of -21.57 dB is reached when applying a rotation of 38 degrees, at which point the corresponding mean grating lobe level is -59.43 dB. The lowest mean grating lobe level is -59.58 dB, at a rotation angle of 44 degrees, with a corresponding maximum grating lobe level of -17.07 dB.

The difference between the mean grating lobe levels is minimal at the 38-degree and 44-degree rotation, thus selecting the optimal design is recommended based on the maximum grating lobe level. Following this criterion, applying the 38 degree provides the best overall design.

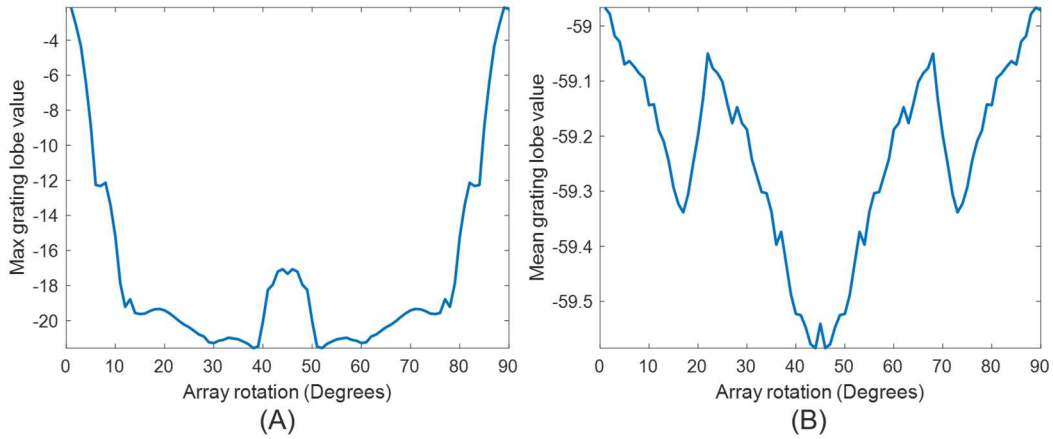

Figure 5. (A) Maximum and (B) mean grating lobe levels from the array directivity calculated for the rotated array optimisation. Y axis units are in dB.

In this work, we have presented an analytical optimization process for 2D laser ultrasonic phased arrays. The work presented here is an important step towards realizing a framework for rapid experimental prototyping of 2D ultrasonic phased arrays. The current work specifically considered the laser ultrasonic directivity patterns and this approach can be easily expanded to consider the

characteristics of other transduction methods, such as piezoelectric transducers. This change in directivity also be achieved in experiment, where utilizing certain approaches can alter the directivity of laser ultrasound. For example, multiple laser beams have been utilized to steer and focus ultrasound [10], or transparent constraining layer can be added to the surface to produce high amplitudes bulk waves to the surface [11]. In future work the experimental framework utilized in [8] will be employed to demonstrate the rapid prototyping capabilities utilizing the optimization process presented in this paper.

Furthermore, while the aim of this work was to establish a phased array optimization framework, a novel ultrasonic phased array design was also presented, the rotated array, which was shown here to outperform the random and the Vernier array -two commonly utilized sparse array designs- in producing both the lowest possible maximum grating lobe and the corresponding mean grating lobe levels. In this work the optimization of this design was limited to testing the amount of rotation applied to the array. In future work the full potential of this design can be explored by considering other optimization parameters, such as applying a Vernier design to the rotated array.

References

[1] Velichko A, Wilcox PD. Defect characterization using two-dimensional arrays. In AIP Conference Proceedings 2011 Jun 23 (Vol. 1335, No. 1, pp. 835-842). American Institute of Physics.

[2] Wooh SC, Shi Y. Optimum beam steering of linear phased arrays. Wave Motion. 1999 Apr 1;29(3):245-65.

[3] Goss SA, Frizzell LA, Kouzmanoff JT, Barich JM, Yang JM. Sparse random ultrasound phased array for focal surgery. IEEE Transactions on Ultrasonics, Ferroelectrics, and Frequency Control. 1996 Nov;43(6):1111-21.

[4] Austeng A, Holm S. Sparse 2-D arrays for 3-D phased array imaging-design methods. IEEE Transactions on Ultrasonics, Ferroelectrics, and Frequency Control. 2002 Aug;49(8):1073-86.

[5] Ramadas SN, Jackson JC, Dziewierz J, O'Leary R, Gachagan A. Application of conformal map theory for design of 2-D ultrasonic array structure for NDT imaging application: A feasibility study. IEEE Transactions on Ultrasonics, Ferroelectrics, and Frequency Control. 2014 Feb 25;61(3):496-504.

[6] Stratoudaki T, Clark M, Wilcox PD. Laser induced ultrasonic phased array using full matrix capture data acquisition and total focusing method. Optics Express. 2016 Sep 19;24(19):21921-38.

[7] Lukacs P, Davis G, Stratoudaki T, Javadi Y, Pierce G, Gachagan A. Remote, volumetric ultrasonic imaging of defects using two-dimensional laser induced phased arrays. In Quantitative Nondestructive Evaluation 2021 Jul 28 (Vol. 85529, p. V001T18A001). American Society of Mechanical Engineers.

[8] Lukacs P, Davis G, Pieris D, Gachagan A, Stratoudaki T. Grating Lobe Suppression Through Novel, Sparse Laser Induced Phased Array Design. In 2022 IEEE International Ultrasonics Symposium (IUS) 2022 Oct 10 (pp. 1-4). IEEE.

[9] Holmes C, Drinkwater BW, Wilcox PD. Post-processing of the full matrix of ultrasonic transmit–receive array data for non-destructive evaluation. NDT & E International. 2005 Dec 1;38(8):701-11.

[10] Pei C, Yi D, Liu T, Kou X, Chen Z. Fully noncontact measurement of inner cracks in thick specimen with fiber-phased-array laser ultrasonic technique. NDT & E International. 2020 Jul 1;113:102273.

[11] Hutchins DA, Dewhurst RJ, Palmer SB. Laser generated ultrasound at modified metal surfaces. Ultrasonics. 1981 May 1;19(3):103-8.